sustainability

MDPI

Article

Smart Wireless Particulate Matter Sensor Node for IoT-Based Strategic Monitoring Tool of Indoor COVID-19 Infection Risk via Airborne Transmission

C. Bambang Dwi Kuncoro [1,*], Cornelia Adristi [2] and Moch Bilal Zaenal Asyikin [1]

[1] Department of Refrigeration, Air Conditioning and Energy Engineering, National Chin-Yi University of Technology, Taichung 41170, Taiwan
[2] Department of Electrical Engineering, Faculty of Engineering, Universitas Indonesia, Depok 16424, Indonesia
* Correspondence: bkuncoro@ncut.edu.tw; Tel.: +886-423924505 (ext. 8274)

Abstract: Indoor and outdoor air pollution are associated with particulate matter concentration of minute size that deeply penetrates the human body and leads to significant problems. These particles led to serious health problems and an increased spread of infection through airborne transmission, especially during the COVID-19 pandemic. Considering the role of particulate matter during the spread of COVID-19, this paper presents a smart wireless sensor node for measuring and monitoring particulate matter concentrations indoors. Data for these concentrations were obtained and used as a risk indicator for airborne COVID-19 transmission. The sensor node was designed to consider air quality monitoring device requirements for indoor applications, such as real-time, continuous, reliable, remote, compact-sized, low-cost, low-power, and accessible. Total energy consumption of the node during measurement and monitoring of particulate matter concentration was minimized using a low-power algorithm and a cloud storage system embedded during software development. Therefore, the sensor node consumed low energy for one cycle of the particulate matter measurement process. This low-power strategy was implemented as a preliminary design for the autonomous sensor node that enables it to integrate with an energy harvester element to harvest energy from ambient (light, heat, airflow) and store energy in the supercapacitor, which extends the sensor node life. Furthermore, the measurement data can be accessed using the Internet of Things and visualized graphically and numerically on a graphical user interface. The test and measurement results showed that the developed sensor node had very small measurement error, which was promising and appropriate for indoor particulate matter concentration measurement and monitoring, while data results were utilized as strategic tools to minimize the risk of airborne COVID-19 transmission.

Keywords: particulate matter; COVID-19; sensor node; Internet of Things; low power

check for updates

Citation: Kuncoro, C.B.D.; Adristi, C.; Asyikin, M.B.Z. Smart Wireless Particulate Matter Sensor Node for IoT-Based Strategic Monitoring Tool of Indoor COVID-19 Infection Risk via Airborne Transmission. *Sustainability* **2022**, *14*, 14433. https://doi.org/10.3390/su142114433

Academic Editors: Ana Fonseca and Nelson Barros

Received: 30 September 2022
Accepted: 30 October 2022
Published: 3 November 2022

Publisher's Note: MDPI stays neutral with regard to jurisdictional claims in published maps and institutional affiliations.

Copyright: © 2022 by the authors. Licensee MDPI, Basel, Switzerland. This article is an open access article distributed under the terms and conditions of the Creative Commons Attribution (CC BY) license (https://creativecommons.org/licenses/by/4.0/).

1. Introduction

The rapid growth of industrial sectors and urbanization have contributed significantly to air pollution. Air pollution has significant impacts on the quality of the environment and harmful effects on human health. In 2019, the World Health Organization (WHO) reported that around 91% of the global population lives in areas with a level of pollution that exceeds the WHO's standard for air quality [1,2]. This condition triggers serious health problems such as stroke, lung cancer, respiratory infections, and chronic obstructive pulmonary disorder. In addition, it causes approximately 7 million premature deaths worldwide every year and a 7% increase in respiratory and cardiovascular diseases [3].

One vital fraction of air pollution can be attributed to particulate matter (PM). This particle matter is very small, with a diameter of less than 10 μm therefore, it can easily enter deeply into the human lung and cause adverse health effects. The effects and hazards on humans caused by this particle have been well understood with the study over the last several decades. Several significant studies presented severe health effects on humans,

such as chronic obstructive pulmonary disorder, cardiac arrhythmia, triggering asthma attacks, coronary heart disease, and premature death [1,4–8].

Particulate matter can be present outdoors and indoors; however, indoor PM concentrations are higher than outdoor [9]. Therefore, indoor PM concentrations significantly contribute to human exposure since 90% of their time and activities are spent indoors [10–12]. Furthermore, most people with chronic health conditions also spend more time indoors. Consequently, indoor PM concentrations will have worse health impacts on room occupants. The WHO noted that household air pollutant exposure causes around 4.3 million people to die annually [13,14].

Indoor PM usually comes from cleaning and smoking tobacco, dust mites, aerosol sprays, pets, insufficient setting gas stoves and furnaces, kindle candles, or burning solid fuel. In many cases, outdoor air infiltration can affect indoor PM concentrations [15]. This infiltration can either increase or decrease indoor PM concentration, depending on the outdoor PM level [16,17].

Since 2020, air pollution has contributed significantly to population mortality [18] and quick transmission of Coronavirus disease 2019 (COVID-19) infection. High exposure to $PM_{2.5}$ and PM_{10} concentrations in a short period is associated with an increased risk of COVID-19 infection [19]. This fact revealed that air pollution is a key factor in spreading COVID-19 infection. Another study presented that an increasing COVID-19 death risk in the United States associates with the average exposure to fine particulate matter ($PM_{2.5}$) over a long period [20]. A COVID-19 death rate increase of 8% is caused by only a 1 $\mu g/m^3$ increase in $PM_{2.5}$ concentration (95% confidence interval [CI]: 2%, 15%). It means that a small increase in $PM_{2.5}$ exposure over a long period contributes to a large increase in the COVID-19 death rate. Other studies concluded that even though the ability of coronavirus to attach to particulate matter has yet to fully understand, continuous exposure to air pollution and related disorders could be a risk factor in defining COVID-19's severity level and the high rate of fatal occurrences [21,22].

Therefore, the measurement of indoor PM concentration is crucial for indoor air quality monitoring and COVID-19 infection transmission risk assessment. To date, the indoor PM concentration can be acquired easily, accurately, in real-time, and quickly using an Indoor Air Quality (IAQ) sensor. Thus, the indoor PM concentration level measurement results can be used as a good indicator and strategic tool to evaluate the risk of COVID-19 infection transmission, especially in an indoor room with crowded occupants or occupants who use their time mostly indoors.

Several studies reported developing and using air quality sensor systems to monitor indoor air pollutants. The authors in [23] conducted a performance examination to evaluate one parameter sensor involving particulate matter (PM), carbon dioxide (CO_2), total volatile organic compounds (TVOC), air temperature, and relative humidity to monitor indoor air quality under controlled air pollution and thermal conditions. Four types of PM sensors with different specifications (measurement range, accuracy, and particle size range) were used in the performance test. The sensor used were Sensirion SPS30, Alphasense OPC-R1, Alphasense OPC-N3, and NovaFitness SDS018. Each sensor was coupled with Arduino Mega to transmit and log-acquired PM data to a personal computer during testing. Eight indoor air pollutant sources, which have a range size of $\leq$0.1 μm (ultrafine particle) to <10 μm (coarse particle) and a concentration range of 2 ppm to 2387 ppm, were used to simulate PM levels in the test chamber. The resting result revealed that the PM sensor could be used to detect the PM concentration change in the range of 0.3 to 2.5 μm. The OPC-R1 type sensor provides the best monitoring result for $PM_{2.5}$, and the OPC-N3 type sensor proved the best measurement for PM_{10}. Another sensor node development in [24] utilized a bare, low-cost PM sensor (HPMA115S0) to monitor a chamber as controlled experiments, including incense, burnt, smoke, and toast particles. An additional instrument used to calculate the measurement was the TSI Scanning Mobility Particle Sizer (SMPS) Model 3938 and Aerodynamic Particle Sizer (APS) model 3321, which shows a variety of coefficients of determination (R_2) averaging from 0.21–0.99 for measuring the $PM_{2.5}$. The device for

indoor environment monitoring is based on Arduino Pro Mini, which has been developed to measure relative humidity, temperature, CO_2 concentration, motion monitoring, and PM concentration [25]. The device called School Monitoring Box (SKOMOBO) has been implemented for IAQ monitoring in the classroom environment. It is equipped with Telaire T9602 for temperature and humidity sensors, SenseAir K30 for a CO_2 sensor, PMS3003 for a PM sensor, and Duinotech XC-4444 (Passive InfraRed (PIR)) sensor module for the motion sensor. The PM sensor can be used to detect PM_{10} in the range from 0 $\mu g/m^3$ to 350 $\mu g/m^3$ under an indoor temperature range of 18 to 28 °C. The device also provides interfaces for external equipment such as a real-time clock module, Wireless Fidelity (Wi-Fi) module, Secure Digital (SD) card module, and LCD (Liquid Crystal Display) screen. The device consumes power of around 2.5 W with an operating voltage of 5 V and a current consumption of 500 mA [26].

A device called Speck was developed in [27] for indoor fine particulate matter measurement applications. It uses an optical-based sensor (DSM501) equipped with an onboard signal processing user interface based on a touchscreen LCD and storage. The device is powered by a Universal Serial Bus (USB) interface that can also be used for data downloading to a personal computer. The display can present $PM_{2.5}$ concentration in $\mu g/m^3$, including a historical data graph in the past hour or 12 h. The device performance has been examined using two professional particle counters (HHPC-6 and HHPC-6+) under two environmental conditions, cooking and frankincense burning. The testing results reveal the Speck device error is less than the error generated between two similar professional devices. A portable monitoring device with an array sensor has been developed for indoor environment quality monitoring applications [28]. The array sensor can measure temperature, humidity, total VOCs, CO_2, $PM_{2.5}$, PM_{10}, carbon monoxide (CO), illuminance, and sound levels. The device is equipped with an Extech for data acquisition and the integrated sensor of HPMA115S0 for the PM sensor, CCS811 for the TVOC sensor, T6713 for the CO_2 sensor, LLC110-102 for the CO sensor, and SHT31 for temperature and humidity sensor. The PM sensor has a range of measurements from 0 to 1000 $\mu g/m^3$ and an accuracy of $\pm$15%. It can measure $PM_{2.5}$ and PM_{10} concentrations. The total dimension of the device is 165 mm $\times$ 105 mm $\times$ 55 mm with a total weight of570 g, including batteries. The device is powered by a 10,000 mAh power bank and consumes a current of 103 mA at 5 V. The authors in [29] present a wireless PM sensor for coarse airborne particulate matter sensing in an indoor environment. The device is based on PPD-20V to detect PM with the size $\geq$ {1, 2.5} μm, and DSM301A sensors can measure PM with the size $\geq$ 0.5 μm. The data from the PM sensor is processed by an ATMega128 microcontroller and transmitted wirelessly to a Linux computer using Digi Xbee every 10 min. The device was calibrated using a GT-526S laser particle counter. The experiment results show that the device could easily detect coarse particles with a size $\geq$ 2.5 μm.

Although the previous development of PM measurement systems and the commercial PM measurement devices described in [30–32] have presented significant advances in the monitoring of indoor air pollutants; however, most of those developed PM sensor nodes/devices do not have the characteristics to meet the requirement for indoor PM concentration measurement and monitoring applications. They tend to have relatively high power consumption, large dimensions, and high prices. Sensor nodes for indoor applications must consider some requirements, such as being compact for simple installation with little space availability, less power usage for long-term operation, accessibility, and low-cost development.

The list of some recent development of IAQ systems for indoor applications and current IAQ monitoring devices are summarized in Tables 1 and 2, respectively.

Table 1. IAQ system developing for indoor air pollutant monitoring application.

Study	Application	Parameter	Sensor Module	Communication Module	Power Consumption	Dimension
Demanega et al. [23], 2020	IAQ monitoring under controlled air pollution and thermal condition	PM, CO_2, TVOC, temperature, and relative humidity	Sensirion SPS30, Alphasense OPC-R1, Alphasense OPC-N3, and NovaFitness SDS018	N/A	N/A	N/A
Zou et al. [24], 2020	IAQ/chamber monitoring.	Incense, burnt, smoke, and toast particle	HPMA115S0	N/A	N/A	N/A
Weyers et al. [25], 2017	IAQ monitoring	PM	SMPS 3938 and APS 3321	Wi-Fi	5 V 500 mA	100 mm × 100 mm × 100 mm
Wang et al. [26], 2017	IAQ monitoring in the classroom environment	Temperature and relative humidity, CO_2, PM, and motion	T9602, SenseAir K30, PMS3003, and Duinotech XC-4444	Wi-Fi	5 V 2.5 Watts	100 mm × 100 mm × 100 mm
Taylor et al. [27], 2015	Indoor fine particulate matter measurement	PM	DSM501	USB, Wi-Fi	5 V 500 mA	114.3 mm × 88.9 mm × 93.98 mm
Tiele et al. [28], 2018	IAQ monitoring	Temperature and relative humidity, TVOCs, CO_2, $PM_{2.5}$, PM_{10}, CO, illuminance, and sound level.	HPMA115S0, CCS811, T6713, LLC110-102, and SHT31	I_2C, UART, SPI	5 V 103 mA	165 mm × 105 mm × 55 mm
Weekly et al. [29], 2013	Coarse airborne particulate matter sensing	PM	PPD-20V and DSM301A	802.15.4 transceiver (Digi XBee series)	5 V 150 mA	120 mm × 100 mm

Table 2. IAQ monitoring devices available on the market.

Sensor Module	Application & Parameter	Power Consumption	Dimension	Communication Configuration	Study
Corvus IAQ monitor	• IAQ monitoring • VOCs, Temperature, Relative Humidity, and Barometric pressure	15 Watts, 12 VDC	68 mm × 176 mm × 123 mm	Mesh wireless network with a frequency of 2.4 MHz	Palmisan et al. [30], 2021
IKAIR	• IAQ monitoring • Temperature, relative humidity, $PM_{2.5}$, and CO_2	6 Watts, 12 VDC	90 mm × 90 mm × 20 mm	Wi-Fi	Yin et al. [31], 2022 Dai et al. [32], 2018

This paper presents a smart wireless particulate matter sensor node for measuring and monitoring indoor $PM_{2.5}$ and PM_{10} concentrations levels. The measurement and analysis of $PM_{2.5}$ and PM_{10} concentrations data were utilized as indicators to minimize the risk of COVID-19 infection airborne transmission in an indoor environment. The sensor node was designed to provide continuous, accurate, and real-time indoor $PM_{2.5}$ and PM_{10} concentrations data that can be accessed easily, everywhere and anytime, and remotely using a graphical user interface on a monitoring terminal (personal computer/laptop) in an Internet of Things (IoT) system. A power strategy was applied to minimize the total energy consumption of the sensor node during PM concentration data measurement and monitoring. In addition to the usage of low-power components, a low-power algorithm was embedded to drive the sensor node works with low-power consumption in one cycle of $PM_{2.5}$ and PM_{10} concentration data measurement (initialization, sensing, $PM_{2.5}$ transmitting, PM_{10} transmitting, and sleep mode). Cloud storage was also used to store the sensing data while reducing the total power consumption of the overall system, which cannot be achieved if the built sensor node relies on a commercial data logger.

2. Materials and Methods

2.1. COVID-19 Infection Indoor Transmission

Several studies revealed COVID-19 infection in humans spread mainly through direct contact with an infected person, droplet transmission (large droplet) through virus-laden droplets from the infected person's coughing, speaking or sneezing, and airborne transmission through small microdroplets (aerosol) spreads over a distance up to several meters from infected person's exhalation [33–37].

In the context of COVID-19 infection through airborne and droplet transmission, a number of studies present the fact that air pollution also has a role in airborne COVID-19 infection transmission. An increase in only 1 $\mu g/m^3$ of $PM_{2.5}$ in long-term exposure is related to an increase of 8% in the mortality rate of COVID-19 in the United States [20]. In the Netherlands, in a case study in 355 municipalities, an increase of 1 $\mu g/m^3$ of $PM_{2.5}$ concentration is related to an increase in COVID-19 cases between 9.4 and 15.1%, hospitality cases between 2.9 and 4.4%, and death cases between 2.2 and 3.6% [38]. Another study proves that Severe Acute Respiratory Syndrome-Coronavirus-2 (SARS-CoV-2) ribonucleic acid (RNA) was found on airborne $PM_{2.5}$ and PM_{10} during high levels of pollution in the most infected COVID-19 areas in the Bergamo Province of Italy [39].

In many cases, air pollution, including particulate matter, is present in aerosols. Aerosols are micron-sized particles that effortlessly float in the air due to their light weight. During the COVID-19 pandemic, the availability of this particle became more dangerous because a "corona" of mucins/proteoglycans is possibly introduced in microdroplets (aerosol) from the infected person's coughing, speaking, or sneezing. Therefore, the aerosol could easily spread SARS-CoV-2 through the air or the surfaces since it can bind small

particulate [40]. Several studies have also found that SARS-CoV-2 could be carried and spread by particulate matter through aerosol [20,38,39].

The spreading of SARS-CoV-2 is faster in an indoor area with an HVAC (Heating, Ventilating, and Air Conditioning) system. The SARS-CoV-2-contained aerosol can remain floating in the air for up to eight hours; thus, it can circulate in the vent, ductwork, and inside the room. Several studies have been conducted to determine how HVAC systems influence the proliferation of microorganisms, such as viruses, in occupied spaces [41]. Figure 1 illustrates the risk potential of airborne transmission of the SARS-CoV-2 virus in a room equipped with an HVAC system. If the person infected with SARS-CoV-2 is coughing in one area indoors, another person within the building that shares the same HVAC system is more likely to be infected.

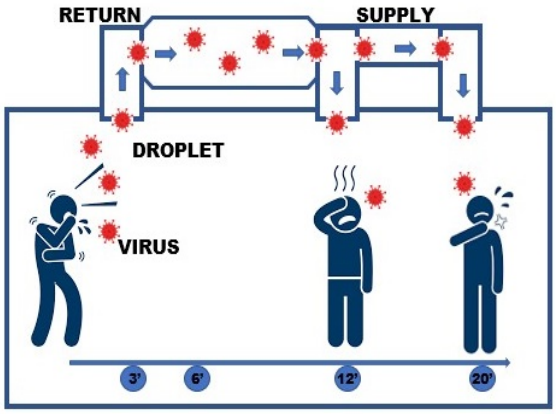


Figure 1. COVID-19 transmission in an indoor environment equipped HVAC system.

2.2. Particulate Matter (PM)

A compound of liquid droplets and solid particles found in the air is called particulate matter (also known as particle pollution). The samples of big particles that can be looked at directly are dust, grime, soot, and smoke, but others are too small to see. Therefore, it only can be detected by an electron microscope. The most common type of PM is PM_{10} particles, inhalable particles less than 10 µm in diameter. Another is $PM_{2.5}$ particles, fine inhalable particles with a diameter of less than 2.5 µm [2].

Both PM_{10} and $PM_{2.5}$ are formed as solid matter from natural sources such as dust, soil, and anthropic activities. These microscopic particles are easily spread throughout nature, flow with the wind, and cannot be looked at directly. Yet, they are responsible for the haze that commonly appears in the sky over polluted places. PM is mostly formed in an outdoor environment, then spreads indoors through doors, windows, or vents. This outdoor PM is commonly called outdoor air pollutants. Several materials, which frequently consist of an outdoor PM_{10} and $PM_{2.5}$ in ambient air, are presented in Figure 2.

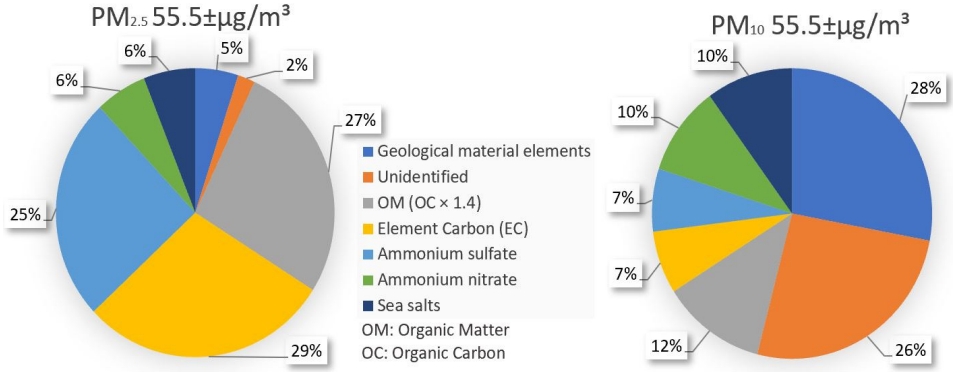


Figure 2. Outdoor particulate matter general composition.

Meanwhile, the PM formed indoors is composed of different materials. Although it's shared the same characteristics as solid matter, it can consist of anthropogenic and natural biogenic elements (such as skin cells, human and animal hair, plant pollen, and textile fibers) as well as a variety of other materials found in the surrounding environment in indoor spaces [42]. These particles cannot be looked at directly, yet they are responsible for the haze that commonly appears in the sky over polluted places. Because these particles are so small, they remain suspended in the indoor air environment for a long time and are difficult to remove using filters.

Compared to outdoor PM, indoor PM contains common and distinctive contaminants. For example, indoor PM can form pollutants like emissions from industrial pollutants. These hazardous material pollutants are the sources of Indoor Air Pollution (IAP). There are classifications such as chemical, physical, biological, and radiological, and the pollutants can be categorized based on their nature. Solid materials such as dust and sand are classified as physical pollution. In contrast, microorganisms such as bacteria, mold spores, algae, and viruses are classified as biological pollutants, but radon is categorized as a radiological pollutant [43]. The PM source from the indoor environment is illustrated in Figure 3.

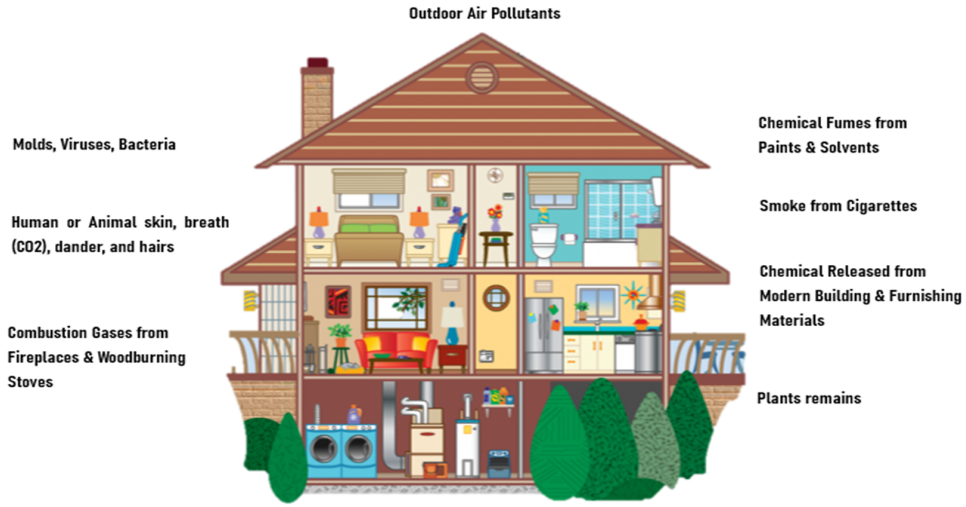


Figure 3. The indoor sources of particulate matter.

2.3. Proposed PM Sensor Node

2.3.1. Design Overview

The architecture of the proposed PM sensor node is shown in Figure 4. The proposed sensor node was designed for indoor PM concentration measurement purposes. A microcontroller unit was applied as a processor of the sensor node to process the measured data from the air quality sensor and control all sensor node components' operations. A PM sensor that works as an air quality sensor was integrated with the microcontroller to collect indoor $PM_{2.5}$ and PM_{10} concentrations. The acquired PM data was sent to the cloud over an IoT system using a Wi-Fi unit for further data processing and analysis. The sensor node is equipped with a power unit to provide stable power for sensor node operation. The main power of the sensor node is a rechargeable power storage (supercapacitor/Li-ion battery/Li-po battery) that acquires energy from an external energy source, either a wall power supply adapter or ambient energy using a battery charger unit. The power storage delivers regulated voltage to the sensor node through the regulator unit.

The compact design was considered to meet the indoor air quality monitoring application requirement, meaning the sensor should be easy to install and occupy a small space for installation. The components for this sensor node are also specifically chosen with low power consumption. Moreover, a low-power mode algorithm was applied to the system during PM data measurement and the use of an IoT system for future data processing. Both the components and the algorithm are applied to ensure the system can reduce the total

energy consumption of the sensor node. IoT systems paired with the sensor node store sensory data while lowering the total system power consumption, which cannot be applied using a commercial data logger. Furthermore, the IoT system allows users to access and monitor sensor data anywhere and anytime. The design of the current sensor node can be integrated with a micro-energy harvester as a power source in the future development of autonomous PM sensor nodes using the proposed low-power strategy.

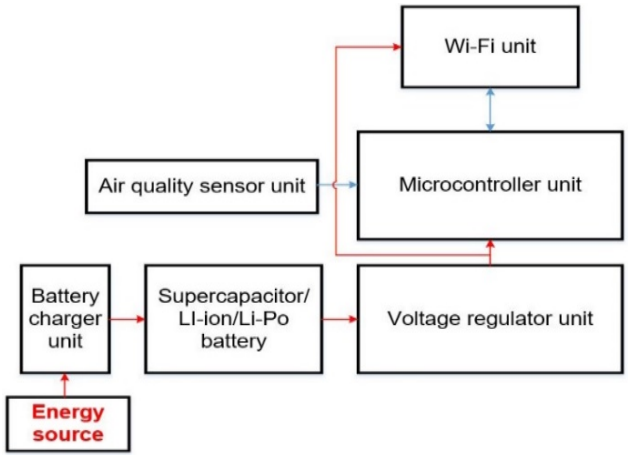


Figure 4. IAQ sensor node architecture.

2.3.2. Hardware Design

The sensor node components were integrated into a single unit based on the node architecture in Figure 4 to make the device compact. The node design and the main components are described as follows.

A. The node board layout

The sensor node main board was designed using Altium Designer software. A compact sensor node design was realized on a two-layer Printed Circuit Board (PCB) with a board dimension of 25 mm × 50 mm, as shown in Figure 5. The surface mount device (SMD) components type was chosen to meet compact and small-size sensor node features.

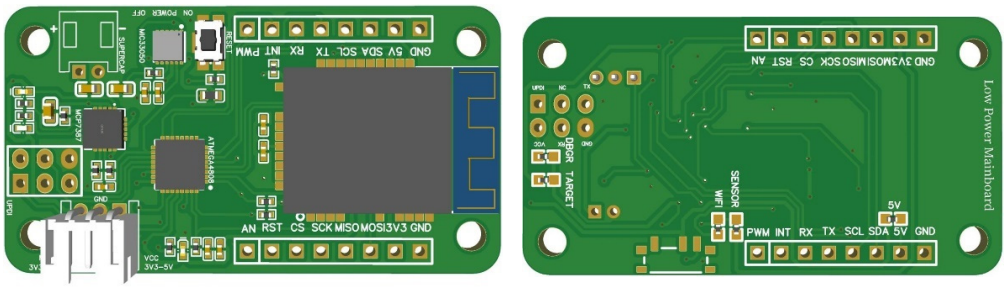


Figure 5. PCB design of IAQ sensor node: (**a**) top layer; (**b**) bottom layer.

All sensor node components, including a microcontroller chip, Wi-Fi module chip, battery charger chip, and voltage regulator chip, were circuited and soldered on the top layer of the PCB. A bus connector was provided on the top layer of the PCB for PM sensor module interconnection. The bottom layer of the PCB was used as a trace for component interconnection. The board also provided a power terminal placed on the top layer of the PCB for power storage (supercapacitor, rechargeable battery) inter-connection. The commercial off-the-shelf (COTS) components were used in the sensor node implementation to reduce costs, as those components are easy to purchase at a low cost.

B. PM sensor

The SPS30 sensor module was integrated with the sensor node board to measure $PM_{2.5}$ and PM_{10} concentrations. Sensorion developed the sensor module based on laser scattering technology that allows PM concentration to be measured with high accuracy, reliability, and resolution [44]. It has small dimensions (41 mm × 41 mm × 12 mm) and is a compact module, as shown in Figure 6.



Figure 6. The PM sensor module.

This sensor module is characterized by a mass concentration precision of ± 10%, and a mass concentration range of 0–1000 µg/m^3. It has more than a 10-year lifetime with a wide range of particle size measurements ($PM_{1.0}$, $PM_{2.5}$, PM_4, and PM_{10}). The measurement outputs are delivered using Inter-Integrated Circuit (I_2C) or Universal Asynchronous Receiver/Transmitter (UART) interfaces. During PM measurement, the sensor operates at a supply voltage range of 4.5–5.5 V with an average supply current of 55 mA and a maximum supply current of 80 mA.

C. The ATMega4808

The ATMega4808 is an eight-bit core of the Advanced Virtual RISC (AVR) family microcontroller with some features, such as running at operating frequencies up to 20 MHz, the memory capacity of Flash up to 48 KB, Static Random Access Memory (SRAM) up to 6 KB, Electrically Erasable Programmable Read Only Memory (EEPROM) up to 256 bytes, and the usage of latest Core Independent Peripherals (CIPs) with the features of low power (advanced peripheral, event system, and intelligent analog peripheral) [45,46]. Additional features are shown in Table 3.

Table 3. The ATMega4808 Feature.

Features	Value
The range of operating voltage	1.8–5.5 V
The range of operating current	
• active mode	1.2 µA–11.4 mA
• idle mode	1.8 µA–2.8 mA
• standby mode	0.7 µA (typical), 16 µA (maximum)
• power-down mode	0.1 µA (typical), 15 µA (maximum)
Analog to Digital Converter (ADC)	
• number	1
• channel	12
• resolution	10 bits
Interface	I_2C, serial peripheral interface (SPI), UART/Universal Synchronous/Asynchronous Receiver/Transmitter (USART)
Package	28- and 32-pin

D. The ATWINC1510

The ATWINC1510 was used to interface with the IoT system. It is a network controller from a microchip characterized by low power consumption and works based on IEEE 802.11 b/g/n IoT network protocols [47]. The module has a small package with dimensions of 21.7 mm × 14.7 mm × 2.1 mm, and is equipped with a switch, power management, low noise amplifier (LNA), power amplifier, and an internal antenna or an external antenna. It can couple with the host controller using either SPI or UART interfacing and minimum resource requirement to perform low-power IoT applications. Its additional features are shown in Table 4.

Table 4. The ATWINC1510 Feature.

Features	Value
Antenna	Printed antenna, a micro co-ax (u.Fl)
Operating frequency	2.412–2.472 MHz
The range of operating voltage	3.0–4.2 V
The operating current	
• Tx	287 mA
• Rx	83 mA
Sleep Mode	4 uA
Flash memory	4 MB
External clock sources	High-speed crystal oscillator (26 MHz)
Package	Quad-Flat No-Leads (QFN)

The embodiment of the Wi-Fi module is shown in Figure 7.



Figure 7. The Wi-Fi module WINC1510.

E. Power storage

The power storage proposed in this system uses a specific component to be compatible with the overall system. This power storage component is specified to be charged from the battery charger units, and there are only two kinds of components able to be used: a supercapacitor and a battery. Therefore, the supercapacitor was chosen compared to the battery due to its better characteristics. The advantages of a supercapacitor involve the recharger cycle life of more than 10^6 cycles, a self-discharge rate of more than 30%, a wide range power density of up to 500 W/m^3, a faster charging time of seconds to minutes, a faster discharging time of less than a few minutes, and the use of simple charging circuits [48]. The proposed system requires a supercapacitor with high capacitance and a voltage of 5 V. Therefore, a certain circuit of several supercapacitors is installed to achieve the right amount of voltage with high capacitance. These supercapacitors are connected in parallel using two homogenous supercapacitors with the specifications of 5.5 V and 5 F. Thus, the total equivalent circuit of the supercapacitor value is 5.5 V 10 F. The features are shown in Table 5.

Table 5. The Supercapacitor Feature.

Features	Value
The lifetime of recharge cycle	$>10^6$ cycles
The rate of self-discharge	30%
Voltage	0 V–2.7 V
The energy density (Wh/m^3)	low (0.8–10)
The power density (W/m^3)	high (400–500)
The range of charging time	Sec–min
The range of discharging time	<a few min
The changing circuit	simple

The series of two units of 5.5 V 5.0 F supercapacitor is shown in Figure 8.

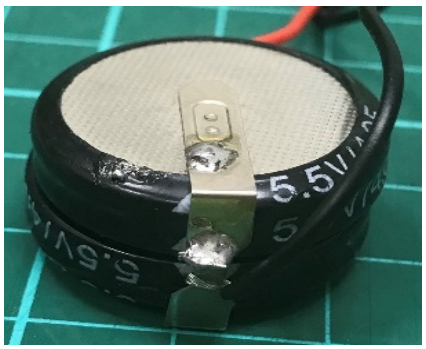


Figure 8. The Supercapacitor.

2.3.3. Software Development

The proposed software in this system was designed to control sensor node activity using a C code-based sensor node software and written using the Arduino Development Environment (IDE). Setup and Loop are the two primary sections of the code. Variable declaration, I/O setup, interface setup, and interface setup are all included in the Setup section. While the Loop section covers the Wi-Fi/internet connection, PM data reading and processing, PM data transfer and logging to the cloud, PM data presentation on the IoT system, and power-down mode. The power-down mode is activated between one cycle of PM data measurement. It is applied to reduce overall sensor node power consumption during the PM measurement process. The Adafruit dashboard developed by Adafruit IO was used to visualize PM data and trends on the terminal monitor. It connects a graphical user interface to the recorded PM data in the cloud of an IoT system (GUI). The program's algorithm is described with the pseudo-code as shown in Algorithm 1.

Algorithm 1 The Logical Flow of Smart Wireless PM Sensor Node

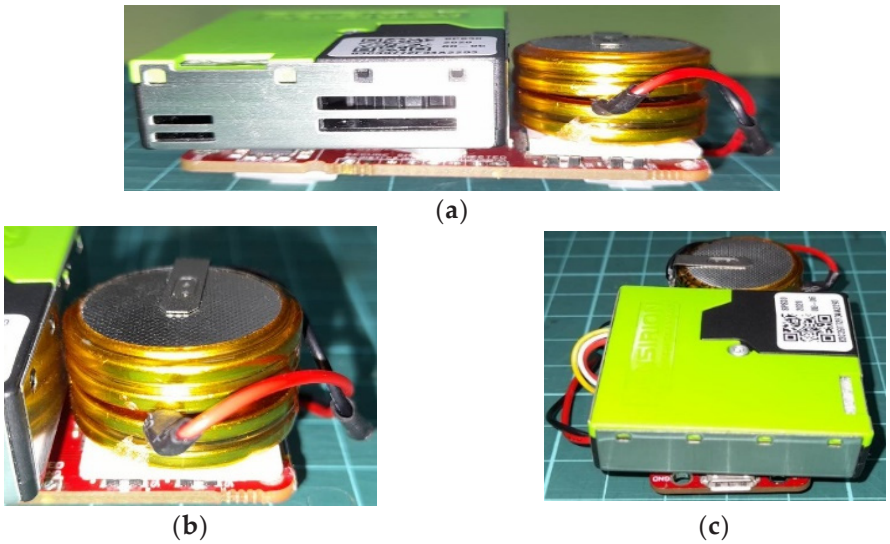
```
Start program sensor node activity while power is ON
Initialize wireless internet connection.
If Wi-Fi is connected successfully:
    Start PM level measurement,
    Process the data of PM,
    Send Measured Data from the sensor to IoT Cloud Interface,
    Print PM data to the IoT page,
    Wait to standby and set a low-power mode until a one-minute cycle is achieved.
Or Else:
    Retry Wireless Connection Internet.
    Return to repeat measuring data.
Stop sensor node activity while power is OFF.
```

3. Result and Discussion

Particulate matter sensor node design was implemented with a compact and small design. In addition, the PM sensor node was validated using calibrated PM measurement device. All design results and testing, including PM reading validation, power consumption calculation, and real-time data visualization, will be discussed in this section.

3.1. Device Implementation

The implementation of the PM sensor node is shown in Figure 9a. The entire system block, including the supercapacitor shown in Figure 9b and the PM sensor (SPS30) shown in Figure 9c, is integrated on a compactly designed mainboard. The size of the prototype system is 60 mm × 41 mm × 13 mm, consisting of a 60 mm × 12 mm mainboard, a 41 mm × 41 mm × 12 mm PM sensor (SPS30), and a supercapacitor 10 V/10 F with the diameter of 30 mm. The small and compact PM sensor node design allows for easy installation, even in small spaces.



(**a**) (**b**) (**c**)

Figure 9. PM sensor node prototype: (**a**) side view; (**b**) supercapacitor; (**c**) top view.

3.2. Graphical User Interface (GUI)

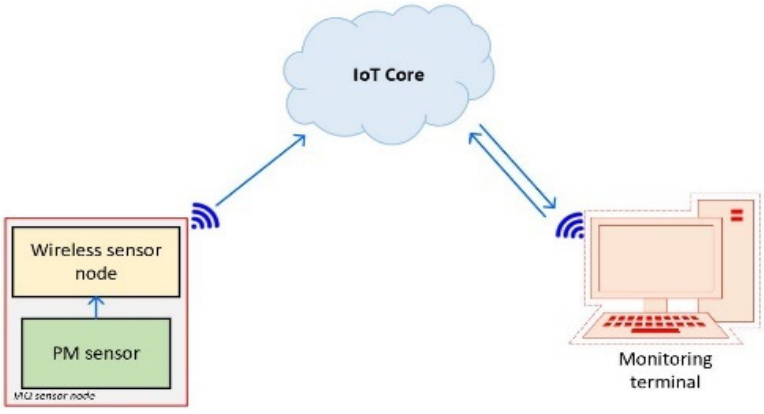
The GUI was implemented using the Adafruit platform, as shown in Figure 10. In general, there are three blocks of data visualization: line chart, gauge, and text log. The line chart block will continuously show graphical data up to the last days. The line chart will help the user to see the PM concentration trend from the PM sensor node readings. Furthermore, the user can analyze the data presented to provide further action. The other block is gauge data visualization that displays the PM concentration's actual value from PM sensor node readings. The data is presented with a measurement range of up to 100 ppm. This is the main indicator to help the user with the actual PM information regarding the environment monitoring target. The last block is text log data visualization that displays the historical communication between the PM sensor node with the IoT core. This block is used during the CO_2 concentration measurement to see the connection between the PM sensor node and the IoT core. The data transfer received by the IoT core will be recorded in the text log, including the time information. This block visualization will easily reveal the lost connection during the experiment. This is very useful to see the PM sensor node performance to maintain the network connection. The dashboard monitor displays the data from PM sensor node readings. However, further action is needed by the user. The dashboard monitor also provides the download data feature that can be accessed as a CSV extension file that can be processed on spreadsheet application software for further analysis.



Figure 10. The dashboard monitoring.

3.3. Functionality Testing

Functionality testing is carried out to see the working functionality of the PM sensor node by the system design. Figure 11a shows the configuration of the system during the functionality testing. The PM sensor node is connected to the IoT core, which uses the Adafruit server. The PM sensor node will be connected to the IoT core through an internet connection and will maintain the connection along the PM sensor node is running. The sensor node is programmed to work in accordance with the algorithm. The PM sensor node is placed on a table inside a room during the testing. The PM sensor node will read the environment PM concentration and transmit the data readings to the IoT core. The user accesses the data stored in the IoT core using a monitoring terminal (a personal computer (PC) or laptop). Figure 11b shows the monitoring dashboard accessed with a PC and displays the PM sensor node readings. All the blocks of data visualization successfully display their functionality. This result confirms that the developed sensor node is successfully running, reading the PM concentration, connecting, and transmitting the data to the IoT core.



(**a**)

Figure 11. *Cont.*



(**b**)

Figure 11. PM sensor functionality testing: (**a**) configuration; (**b**) testing process and result.

3.4. Validating

The PM sensor node reading was validated by comparing the PM sensor node with Particulate Counter SEAT HT-9600 calibrated by TSI DustTrak DRX 8533. Particulate Counter SEAT HT-9600, as a reference measurement device, has an accuracy of ±12% (or ±12 μg/m^3) with a range of measurement from 0 to 1000 μg/m^3.

The configuration of validation is shown in Figure 12a. The PM sensor node and Particulate Counter SEAT HT-9600 were placed in several places: on the table, on the cupboard, in the cupboard, on the chair, and under the table in an indoor environment to measure PM concentration, as shown in Figure 12b. The PM sensor node was also connected to the IoT system. Therefore, the PM sensor node reading data could be monitored on dashboard monitoring, as shown in Figure 12a.



(**a**) (**b**)

Figure 12. Verification process of PM sensor node: (**a**) measurement setup; (**b**) sensor node and validator placement in an indoor environment.

The result of the measurement, which was to validate the PM sensor node, is shown in Table 6. The average error of the PM sensor node measurement is 4.06%, both for the $PM_{2.5}$ and PM_{10} measurement results. It proves the sensor's accuracy compared with the Particulate Counter SEAT HT-9600. Therefore, the PM sensor node can be used to analyze the indoor PM concentration.

Table 6. The Validation Measurement Result.

Sensor Node (ppm)		Validator (ppm)		Error (ppm)		Absolute Percentage Error (%)	
$PM_{2.5}$	PM_{10}	$PM_{2.5}$	PM_{10}	$PM_{2.5}$	PM_{10}	$PM_{2.5}$	PM_{10}
3.14	3.14	3.00	3.00	−0.14	−0.14	4.67	4.67
3.15	3.15	3.00	3.00	−0.15	−0.15	5.00	5.00
3.14	3.14	3.00	3.00	−0.14	−0.14	4.67	4.67
2.84	2.84	3.00	3.00	0.16	0.16	5.33	5.33
2.94	2.94	3.00	3.00	0.06	0.06	2.00	2.00
3.08	3.08	3.00	3.00	−0.08	−0.08	2.67	2.67
Average Error				−0.05	−0.05		
Average Percentage Error						4.06	4.06

3.5. Power Capacity Requirement

In this test, current and time measurements were carried out on each process after one cycle of PM concentration measurement. By knowing these two parameters, the PM sensor node's power consumption and energy capacity requirement can be calculated. In addition, testing was also carried out on power storage. This is conducted to see the ability to charge and discharge power storage to drive the power needs of the PM sensor node.

Based on the PM sensor node design, there are five processes in one cycle of PM concentration measurement: initializing, sensing, $PM_{2.5}$ transmitting, PM_{10} transmitting, and sleep. Each process has its role and function. Therefore, in one cycle, the PM sensor node performs the starting process, reads the PM sensor, sends the $PM_{2.5}$ and PM_{10} data readings, and enables low power mode at predetermined intervals. A detailed description of each process can be seen in Table 7.

Table 7. The PM Sensor Node Working Process.

Process	Description
Initializing	All variable preparation and disable low power mode
Sensing	Sensor node working to measure PM concentration
$PM_{2.5}$ data transmitting	Transmit $PM_{2.5}$ data to the server
PM_{10} data transmitting	Transmit PM_{10} data to the server
Sleep	Enable low-power mode

3.5.1. Current Measurement

The sensor node's current measurement configuration comprises the PM sensor node integrated with a current sensor and external microcontroller, as shown in Figure 13. The 1NA219 sensor was used as a current sensor and connected with Arduino Mega 2560 using an I_2C interface. It also uses a power source from the 5 V power pin of the Arduino Mega 2560 to ensure no interference from other external power sources. The current measurement of the PM sensor node was done by connecting the PM sensor node's main storage (supercapacitor) to the 1NA219 sensor. With this connection, the 1NA219 measured the overall current consumption of the PM sensor node.

The current measurement result of each process can be seen in Figure 14. The initialization process requires a current of 104.9 mA. In this process, all I/O and interfaces of ATMega4808 are initialized. The initialized interface includes the interface used to communicate with the PM sensor and the Wi-Fi module. In addition, the Wi-Fi module network settings are also initialized in this process. In this stage, the PM sensor node has been connected to the internet network. The current consumption increased in the sensing process to

123.86 mA due to the PM sensor (SPS30) started reading the PM concentration. At this stage, the PM sensor generates two output data values, namely the concentration values of $PM_{2.5}$ and PM_{10}. After the PM sensor obtains these two parameters, the PM sensor node will stop the reading process and start transmitting $PM_{2.5}$ and PM_{10} concentration value data to the IoT core in the next stage. The $PM_{2.5}$ transmitting stage requires a current of 131.3 mA, and the PM_{10} transmitting stage requires a current of 120.7 mA. The internet connection and network coverage will determine the current consumption at this stage. This is related to the current consumption needed by the Wi-Fi module, which will increase when the internet connection is bad, and the network coverage is too far. The current measured at this stage is the largest of the entire PM sensor node working process. However, the measured current is significantly reduced to 81.7 mA at the sleep stage. The PM sensor node will activate low-power mode and disable some interfaces on the ATMega4808. At this stage, the measured current is the smallest in the entire PM sensor node working process.

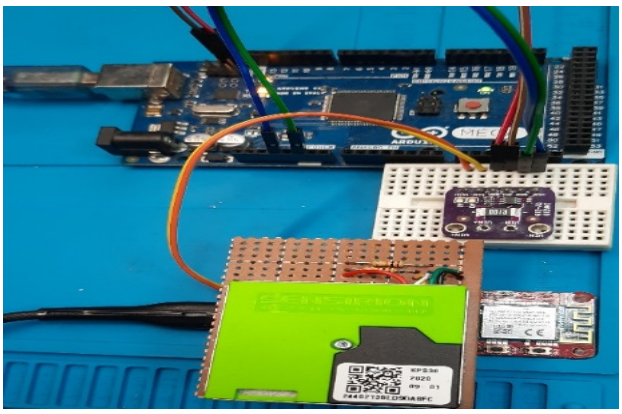


Figure 13. The current measurement process configuration setup.

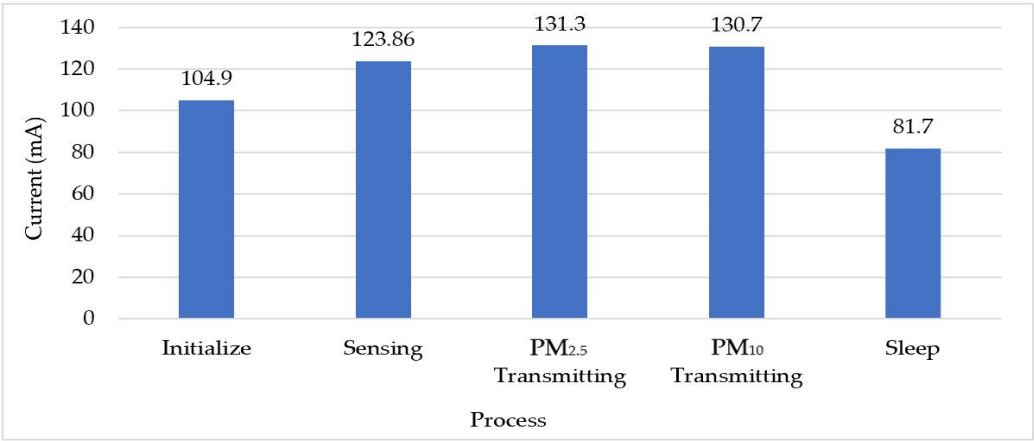


Figure 14. The current measurement results.

3.5.2. Time Consumption

The time measurements were carried out to measure the time requirements for each process in the PM concentration measurement, which is presented in Table 5. The measurement was conducted using a program-based measurement approach. The program measured time consumption based on each process's start time and stop time in one cycle of PM concentration measurement. The measurement result of time consumption is presented in Figure 15. Each time process, including the initialization process, sensing, $PM_{2.5}$ transmitting, and PM_{10} transmitting are 662 ms, 28 ms, 1716.6 ms, and 1354 ms, respectively. In the initialization and sensing processes, the time required is relatively fast compared to the transmitting process due to the operating cycle of ATMega4808 running up to 20 MHz.

While transmitting, the time required will be related to the internet connection. A better internet connection takes a faster time to transmit the $PM_{2.5}$ or PM_{10} data.

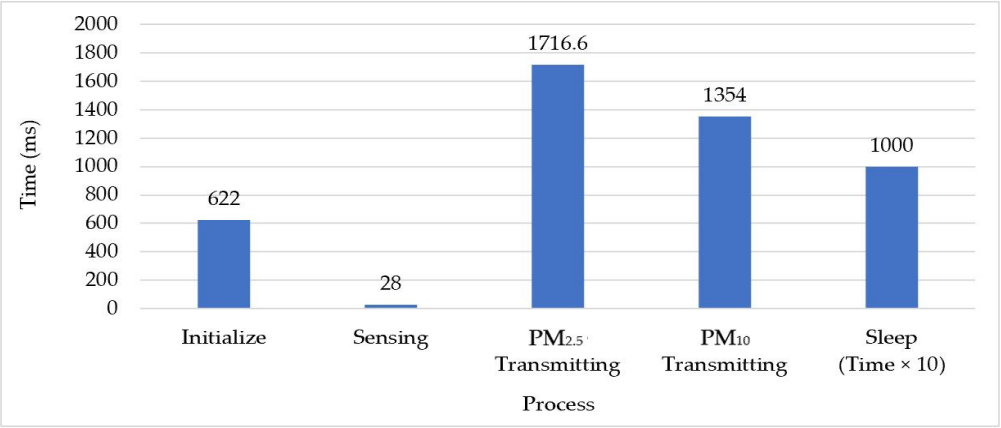


Figure 15. The time consumption.

The time in the sleep process is a predetermined time. The sleep process is used as the time interval for the PM sensor node to repeat the measurement cycle from initialization. Therefore, this process changes the PM sensor node to a low-power mode. It aims to reduce current consumption. The predetermined time was set at 10,000 ms. The timing was chosen to consider that the concentrations of $PM_{2.5}$ and PM_{10} did not change significantly in a short time. Therefore, the timing can still provide $PM_{2.5}$ and PM_{10} reading the information in real-time but consuming low power.

3.5.3. The Energy Capacity

The energy capacity estimates the energy usage of the PM sensor node in one work cycle, including initialization, sensing, $PM_{2.5}$ transmitting, PM_{10} transmitting, and sleep. The energy capacity can be calculated using the current and time measurements data. With the PM sensor node working voltage at 4.68 V, the energy capacity for each process in one cycle of PM concentration measurement is presented in Table 8. The smallest energy capacity is found in the sensing process, requiring only 0.0045 m Wh of power storage. In comparison, the sleep process consumes the largest energy consumption of 1.0621 mWh. The two processes have a very significant difference in energy capacity required because it is influenced by the time required for the two processes also have a very substantial difference. One cycle of PM concentration measurement requires an energy capacity of 1.68 mWh. The system's design requires a small energy capacity is very important. PM sensor node with low power consumption is very supportive of achieving autonomous PM sensor nodes in the future with the addition of an energy harvesting generator.

Table 8. The Energy Capacity.

Process	Voltage (V)	Current (mA)	Power (mW)	Time (ms)	Energy Capacity Required (mWh)
Initializing	4.68	104.9	490.93	662	0.0903
Sensing	4.68	123.86	579.66	28	0.0045
$PM_{2.5}$ transmitting	4.68	131.3	614.48	1716.6	0.293
PM_{10} transmitting	4.68	130.7	611.68	1354	0.23
Sleep	4.68	81.7	382.36	10,000	1.0621
Total Energy Required (one cycle)					1.68

The percentage of power capacity requirement percentage is shown in Figure 16. The biggest part of the power consumption is 63.22% for sleep mode, 17.44% for $PM_{2.5}$ transmitting, 13.69% for PM_{10} transmitting, 5.37% for sensing, and 0.27% for initializing.

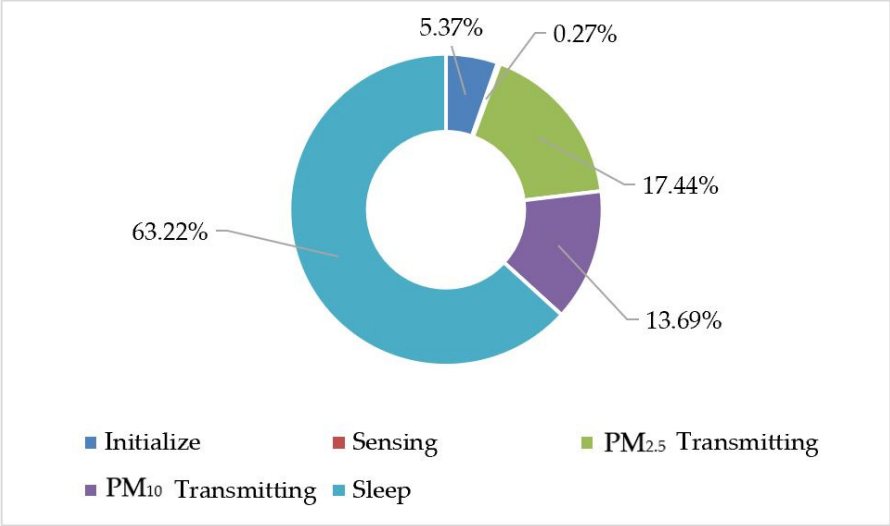


Figure 16. The power capacity requirement percentage.

3.5.4. Power Storage Testing

The PM sensor node uses a power storage supercapacitor with a specification of 5.5 V/10 F. In this test, observations were conducted on the charging and discharging processes of the supercapacitor. The PM sensor node is connected to a DC 5 V power supply during the charging process. Based on Figure 17, the supercapacitor charging process takes 16 s with an initial voltage of 4.5 V to a final voltage of 4.96 V. After the charging process is complete, the power supply connected to the PM sensor node is then disconnected. The PM sensor node will use the supercapacitor as the main power. Using power storage in the supercapacitor to run the PM sensor node is a discharging process. During the discharging process, the power capacity of the supercapacitor will decrease. With an initial voltage of 4.96 V to a final voltage of 4.5 V, the supercapacitor can drive power for the PM sensor node for 10 s. In further research, the supercapacitor capacity can be increased to make the discharging process longer. Moreover, the supercapacitor charging process will be carried out using an energy-harvesting generator. Thus, the PM sensor node can use energy harvesting to drive the PM sensor node.

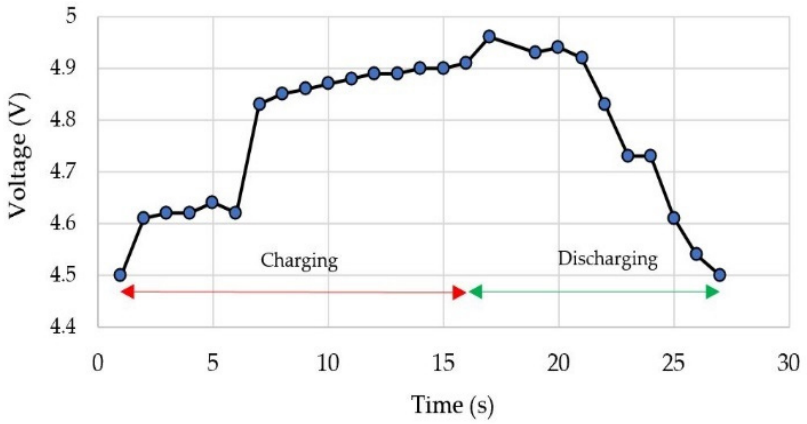


Figure 17. The charging and discharging process.

3.6. PM Concentration Measurement Experiment

3.6.1. Configuration

The configuration of the system is shown in Figure 18. It started measuring PM concentration by the sensor node, which was connected to the Wi-Fi, then the data was sent to the IoT core in the cloud. Therefore, Adafruit can take the data from the IoT core for

monitoring to be analyzed, and our equation was defined before the equation appeared or immediately following.

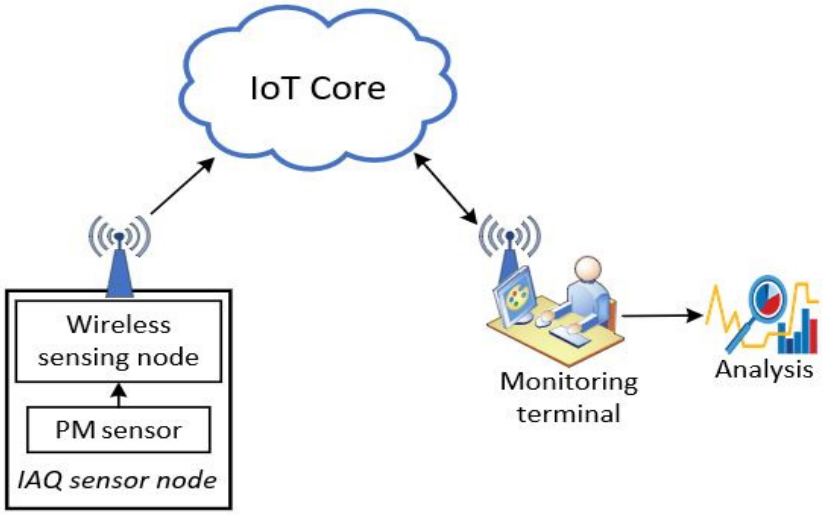


Figure 18. The PM sensor node testing setup.

3.6.2. Measurement Result

The measurements were taken in an indoor room for four days and outdoors for four days. The result is shown in Figure 19a for the measurements in an indoor space and Figure 19b for the outdoor measurements. The results showed that the PM sensor node and the monitoring system can be operated successfully both indoors and outdoors. The sensor node can read PM concentration in an indoor room and an outdoor room and send the data to the cloud. The data was received on the Adafruit platform for displaying the data to be monitored on the monitoring dashboard. The range of PM concentrations level for four days on graphical data is 0 to 25 ppm.



(**a**)

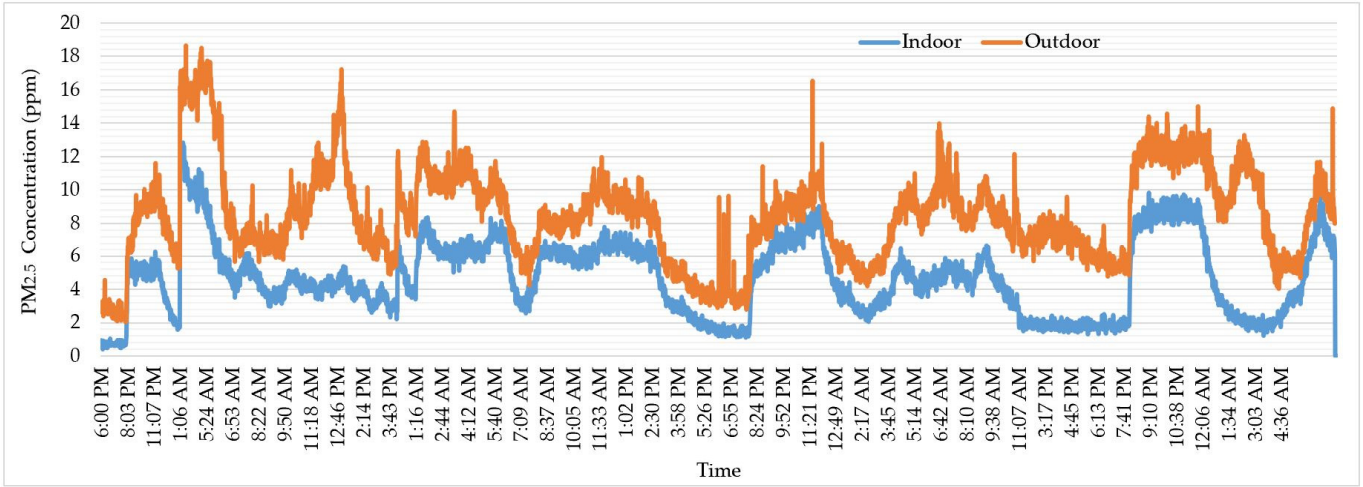
Figure 19. *Cont.*



(**b**)

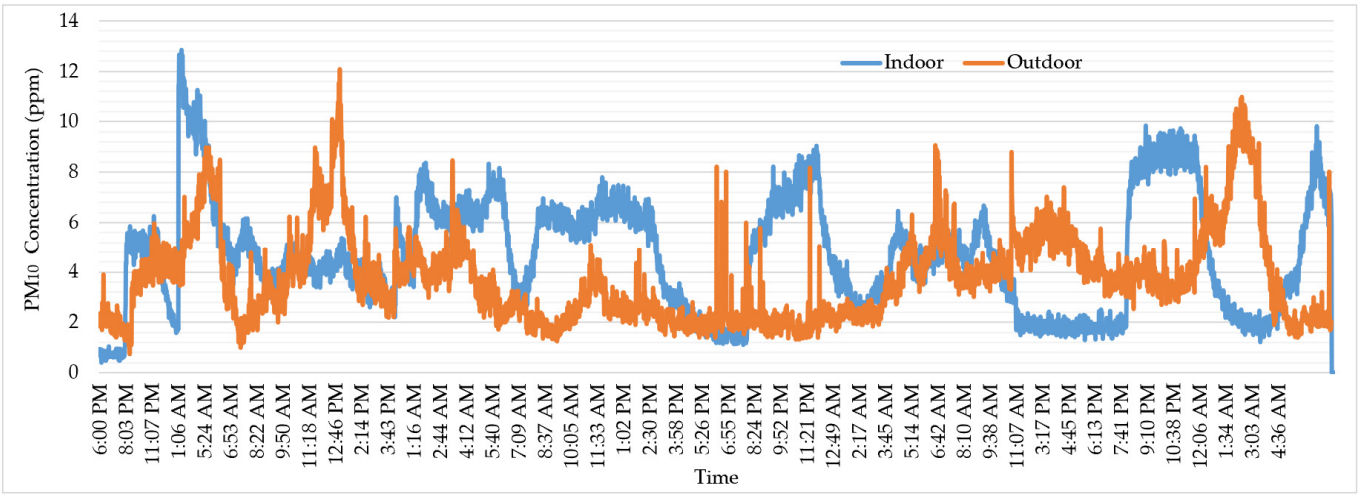
Figure 19. The monitoring dashboard: (**a**) indoor; (**b**) outdoor.

The continuous PM sensor node reading formed trend-historical data that could be downloaded as a CSV file. Later, the downloaded data was refined in chart form with a different type of specific PM, as shown in Figure 20a for $PM_{2.5}$ and Figure 20b for PM_{10}. The chart shows the downloaded data after four days of measurements from the PM sensor. The range of $PM_{2.5}$ concentration levels in an indoor environment for four days was 0.40–12.84 ppm, while for the outdoor environment was 0.40–12.84 ppm. As for the PM_{10}, the measured value was not much different for indoor and outdoor environments compared with the $PM_{2.5}$. The average of three days of both $PM_{2.5}$ and PM_{10} in an indoor environment is 4.70 ppm, while in an outdoor environment is 3.77 ppm.



(**a**)

Figure 20. *Cont.*



(**b**)

Figure 20. The monitored data: (**a**) $PM_{2.5}$; (**b**) PM_{10}.

The measured value of PM depends on many factors, such as the ventilation setting condition, the number of indoor inhabitants, the activities of the people, etc. Based on the data of this research, both $PM_{2.5}$ and PM_{10} in an indoor environment have higher values than those in an outdoor environment.

4. Conclusions

The smart-wireless PM sensor node was built from integrated components and programmed to work according to the proposed design. Using low-cost and easily acquired components on the market, the compact design is achieved with 60 mm × 41 mm × 13 mm. In one cycle of PM level measurement, the system could operate within a very short time, around 13 s for initializing, data sensing, transmitting, and a sleep mode. With the low power consumption of the sensor node components and algorithm, the total power consumption for a single data measurement cycle was 1.7532 mWh. The power storage of this system consists of parallel supercapacitors with a total value of 5.5 V and a capacity of 10 F, which can be autonomously active for 25 s and can be prolonged since it can be recharged over time.

Furthermore, this power storage recharge system can be further improved by harvesting the indoor ambient energy from several sources, such as indoor ambient temperature, artificial light, air-flow rate, and apparatus heat source using the micro-energy harvester. This energy can be used to prolong sensor nodes for long-term operations toward an autonomous sensor node, which is in further development. The accuracy of the sensor node measurement was validated with a relatively low measurement error of 4.06%. During the measurement experiment, both $PM_{2.5}$ and PM_{10} concentration levels were held outdoors and indoors within an hour, and the sensor node can provide real-time and continuous data measurement. The numerical value of ppm and the graphical chart for both $PM_{2.5}$ and PM_{10} is available to be accessed by the user in the IoT graphical user interface.

Author Contributions: Conceptualization, C.B.D.K.; methodology, C.B.D.K. and C.A.; formal analysis, C.A. and M.B.Z.A.; investigation, C.A. and M.B.Z.A.; supervision, C.B.D.K.; resources, C.B.D.K.; writing—original draft preparation, C.A. and M.B.Z.A.; writing—review and editing, C.B.D.K. All authors have read and agreed to the published version of the manuscript.

Funding: This research funding by the Ministry of Science and Technology of Taiwan (MOST: 110-2222-E-167-003-MY3).

Institutional Review Board Statement: Not applicable.

Informed Consent Statement: Not applicable.

Data Availability Statement: The data presented in this study are available at the request of the corresponding author.

Acknowledgments: The authors would like to thank the Ministry of Science and Technology of Taiwan for funding support and the Refrigeration, Air Conditioning, and Energy Engineering Department of the National Chin-Yi University of Technology, Taiwan, for help with the system design.

Conflicts of Interest: The authors declare no conflict of interest.

References

1. Anderson, J.O.; Thundiyil, J.G.; Stolbach, A. Clearing the Air: A Review of the Effects of Particulate Matter Air Pollution on Human Health. *J. Med. Toxicol.* **2011**, *8*, 166–175. [CrossRef]
2. World Health Organization. *Who Guidelines for Indoor Air Quality: Selected Pollutants*; WHO: Copenhagen, Denmark, 2010; ISBN 978-92-890-0213-4.
3. Jiang, X.-Q.; Mei, X.-D.; Feng, D. Air pollution and chronic airway diseases: What should people know and do? *J. Thorac. Dis.* **2016**, *8*, E31–E40. [CrossRef]
4. Pope, C.A., III; Dockery, D.W. Health Effects of Fine Particulate Air Pollution: Lines that Connect. *J. Air Waste Manag. Assoc.* **2006**, *56*, 709–742. [CrossRef]
5. Pope, C.A. Epidemiology of fine particulate air pollution and human health: Biologic mechanisms and who's at risk? *Environ. Health Perspect.* **2000**, *108*, 713–723. [CrossRef]
6. Brook, R.D.; Franklin, B.; Cascio, W.; Hong, Y.L.; Howard, G.; Lipsett, M.; Luepker, R.; Mittleman, M.; Samet, J.; Smith, S.C.; et al. Air pollution and cardiovascular disease—A statement for healthcare professionals from the expert panel on population and prevention science of the American Heart Association. *Circulation* **2004**, *109*, 2655–2671. [CrossRef]
7. Sørensen, M.; Daneshvar, B.; Hansen, M.; Dragsted, L.O.; Hertel, O.; Knudsen, L.; Loft, S. Personal PM2.5 Exposure and Markers of Oxidative Stress in Blood. *Environ. Health Perspect.* **2002**, *111*, 161–165. [CrossRef]
8. Brook, R.D.; Rajagopalan, S.; Pope, C.A., 3rd; Brook, J.R.; Bhatnagar, A.; Diez-Roux, A.V.; Holguin, F.; Hong, Y.; Luepker, R.V.; Mittleman, M.A.; et al. Particulate Matter Air Pollution and Cardiovascular Disease: An update to the scientific statement from the american heart association. *Circulation* **2010**, *121*, 2331–2378. [CrossRef]
9. Klepeis, N.E.; Hughes, S.; Edwards, R.D.; Allen, T.; Johnson, M.; Chowdhury, Z.; Smith, K.R.; Boman-Davis, M.; Bellettiere, J.; Hovell, M.F. Promoting Smoke-Free Homes: A Novel Behavioral Intervention Using Real-Time Audio-Visual Feedback on Airborne Particle Levels. *PLoS ONE* **2013**, *8*, e73251. [CrossRef]
10. Spengler, J.D.; Sexton, K. Indoor Air Pollution: A Public Health Perspective. *Science* **1983**, *221*, 9–17. [CrossRef]
11. Zhang, J.F.; Smith, K.R. Indoor air pollution: A global health concern. *Br. Med. Bull.* **2003**, *68*, 209–225. [CrossRef]
12. Zhu, Y.; Yang, L.; Meng, C.; Yuan, Q.; Yan, C.; Dong, C.; Sui, X.; Yao, L.; Yang, F.; Lu, Y.; et al. Indoor/outdoor relationships and diurnal/nocturnal variations in water-soluble ion and PAH concentrations in the atmospheric PM2.5 of a business office area in Jinan, a heavily polluted city in China. *Atmos. Res.* **2015**, *153*, 276–285. [CrossRef]
13. Burnett, R.T.; Pope, C.A., III; Ezzati, M.; Olives, C.; Lim, S.S.; Mehta, S.; Shin, H.H.; Singh, G.; Hubbell, B.; Brauer, M.; et al. An Integrated Risk Function for Estimating the Global Burden of Disease Attributable to Ambient Fine Particulate Matter Exposure. *Environ. Health Perspect.* **2014**, *122*, 397–403. [CrossRef]
14. Shaddick, G.; Thomas, M.; Mudu, P.; Ruggeri, G.; Gumy, S. Half the World's Population Are Exposed to Increasing Air Pollution. *NPJ Clim. Atmos. Sci.* **2020**, *3*, 23. [CrossRef]
15. Goyal, R.; Kumar, P. Indoor–outdoor concentrations of particulate matter in nine microenvironments of a mix-use commercial building in megacity Delhi. *Air Qual. Atmos. Health* **2013**, *6*, 747–757. [CrossRef]
16. Morawska, L.; He, C.; Hitchins, J.; Gilbert, D.; Parappukkaran, S. The relationship between indoor and outdoor airborne particles in the residential environment. *Atmos. Environ.* **2001**, *35*, 3463–3473. [CrossRef]
17. Kumar, P.; Morawska, L. Energy-Pollution Nexus for Urban Buildings. *Environ. Sci. Technol.* **2013**, *47*, 7591–7592. [CrossRef]
18. Ogen, Y. Assessing nitrogen dioxide (NO2) levels as a contributing factor to the coronavirus (COVID-19) fatality rate. *Sci. Total. Environ.* **2020**, *726*, 138605. [CrossRef]
19. Zhu, Y.; Xie, J.; Huang, F.; Cao, L. Association between short-term exposure to air pollution and COVID-19 infection: Evidence from China. *Sci. Total Environ.* **2020**, *727*, 138704. [CrossRef]
20. Wu, X.; Nethery, R.C.; Sabath, M.B.; Braun, D.; Dominici, F. Exposure to Air Pollution and COVID-19 Mortality in the United States: A Nationwide Cross-Sectional Study. *Epidemiology* **2020**.
21. Chen, H.; Guo, J.; Wang, C.; Luo, F.; Yu, X.; Zhang, W.; Li, J.; Zhao, D.; Xu, D.; Gong, Q.; et al. Clinical characteristics and intrauterine vertical transmission potential of COVID-19 infection in nine pregnant women: A retrospective review of medical records. *Lancet* **2020**, *395*, 809–815. [CrossRef]
22. Wang, D.; Hu, B.; Hu, C.; Zhu, F.; Liu, X.; Zhang, J.; Wang, B.; Xiang, H.; Cheng, Z.; Xiong, Y.; et al. Clinical Characteristics of 138 Hospitalized Patients With 2019 Novel Coronavirus—Infected Pneumonia in Wuhan, China. *JAMA* **2020**, *323*, 1061–1069. [CrossRef]
23. Demanega, I.; Mujan, I.; Singer, B.C.; Anđelković, A.S.; Babich, F.; Licina, D. Performance assessment of low-cost environmental monitors and single sensors under variable indoor air quality and thermal conditions. *Build. Environ.* **2020**, *187*, 107415. [CrossRef]

24. Zou, Y.; Young, M.; Chen, J.; Liu, J.; May, A.; Clark, J.D. Examining the functional range of commercially available low-cost airborne particle sensors and consequences for monitoring of indoor air quality in residences. *Indoor Air* **2019**, *30*, 213–234. [CrossRef]
25. Weyers, R.; Jang-Jaccard, J.; Moses, A.; Wang, Y.; Boulic, M.; Chitty, C.; Phipps, R.; Cunningham, C. Low-Cost Indoor Air Quality (IAQ) Platform for Healthier Classrooms in New Zealand: Engineering Issues. In Proceedings of the 2017 4th Asia-Pacific World Congress on Computer Science and Engineering (APWC on CSE), Nadi, Fiji, 11–13 December 2017; pp. 208–215.
26. Wang, Y.; Boulic, M.; Phipps, R.; Chitty, C.; Moses, A.; Weyers, R.; Jang-Jaccard, J.; Olivares, G.; Ponder-Sutton, A.; Cunningham, C. Integrating Open-Source Technologies to Build a School Indoor Air Quality Monitoring Box (SKOMOBO). In Proceedings of the 2017 4th Asia-Pacific World Congress on Computer Science and Engineering (APWC on CSE), Nadi, Fiji, 11–13 December 2017; pp. 216–223.
27. Taylor, M.D. *A Low-Cost Particle Counter and Signal Processing Method for Indoor Air Pollution*; Nourbakhsh, I.R., Ed.; WIT Press: València, Spain, 2015; pp. 337–348. [CrossRef]
28. Tiele, A.; Esfahani, S.; Covington, J. Design and Development of a Low-Cost, Portable Monitoring Device for Indoor Environment Quality. *J. Sens.* **2018**, *2018*, 1–14. [CrossRef]
29. Weekly, K.; Rim, D.; Zhang, L.; Bayen, A.M.; Nazaroff, W.W.; Spanos, C.J. Low-Cost Coarse Airborne Particulate Matter Sensing for Indoor Occupancy Detection. In Proceedings of the 2013 IEEE International Conference on Automation Science and Engineering (CASE), Madison, WI, USA, 17–20 August 2013; pp. 32–37.
30. Palmisani, J.; Di Gilio, A.; Viana, M.; de Gennaro, G.; Ferro, A. Indoor air quality evaluation in oncology units at two European hospitals: Low-cost sensors for TVOCs, PM2.5 and CO2 real-time monitoring. *Build. Environ.* **2021**, *205*, 108237. [CrossRef]
31. Yin, H.; Zhai, X.; Ning, Y.; Li, Z.; Ma, Z.; Wang, X.; Li, A. Online monitoring of PM2.5 and CO_2 in residential buildings under different ventilation modes in Xi'an city. *Build. Environ.* **2021**, *207*, 108453. [CrossRef]
32. Dai, X.; Liu, J.; Li, X.; Zhao, L. Long-term monitoring of indoor CO2 and PM2.5 in Chinese homes: Concentrations and their relationships with outdoor environments. *Build. Environ.* **2018**, *144*, 238–247. [CrossRef]
33. Curtius, J.; Granzin, M.; Schrod, J. Testing mobile air purifiers in a school classroom: Reducing the airborne transmission risk for SARS-CoV-2. *Aerosol Sci. Technol.* **2021**, *55*, 586–599. [CrossRef]
34. Drossinos, Y.; Stilianakis, N.I. What aerosol physics tells us about airborne pathogen transmission. *Aerosol Sci. Technol.* **2020**, *54*, 639–643. [CrossRef]
35. Buonanno, G.; Morawska, L.; Stabile, L. Quantitative assessment of the risk of airborne transmission of SARS-CoV-2 infection: Prospective and retrospective applications. *Environ. Int.* **2020**, *145*, 106112. [CrossRef]
36. Miller, S.L.; Nazaroff, W.W.; Jimenez, J.L.; Boerstra, A.; Buonanno, G.; Dancer, S.J.; Kurnitski, J.; Marr, L.C.; Morawska, L.; Noakes, C. Transmission of SARS-CoV-2 by inhalation of respiratory aerosol in the Skagit Valley Chorale superspreading event. *Indoor Air* **2020**, *31*, 314–323. [CrossRef]
37. Morawska, L.; Cao, J. Airborne transmission of SARS-CoV-2: The world should face the reality. *Environ. Int.* **2020**, *139*, 105730. [CrossRef]
38. Cole, M.A.; Ozgen, C.; Strobl, E. Air Pollution Exposure and COVID-19 in Dutch Municipalities. *Environ. Resour. Econ.* **2020**, *76*, 581–610. [CrossRef]
39. Setti, L.; Passarini, F.; De Gennaro, G.; Barbieri, P.; Pallavicini, A.; Ruscio, M.; Piscitelli, P.; Colao, A.; Miani, A. Searching for SARS-COV-2 on Particulate Matter: A Possible Early Indicator of COVID-19 Epidemic Recurrence. *Int. J. Environ. Res. Public Health* **2020**, *17*, 2986. [CrossRef]
40. Farhangrazi, Z.S.; Sancini, G.; Hunter, A.C.; Moghimi, S.M. Airborne Particulate Matter and SARS-CoV-2 Partnership: Virus Hitchhiking, Stabilization and Immune Cell Targeting—A Hypothesis. *Front. Immunol.* **2020**, *11*, 579352. [CrossRef]
41. *Coronavirus Transmission Indoors Via Airborne Particles*; Pure Air Control Services Inc.: Clearwater, FL, USA, 2020; Available online: https://pureaircontrols.com/coronavirus-transmission-indoors-via-airborne-particles/ (accessed on 11 June 2022).
42. Cheng, Y.; Lee, S.; Gu, Z.; Ho, K.; Zhang, Y.; Huang, Y.; Chow, J.C.; Watson, J.G.; Cao, J.; Zhang, R. PM2.5 and PM10-2.5 chemical composition and source apportionment near a Hong Kong roadway. *Particuology* **2015**, *18*, 96–104. [CrossRef]
43. Gopalakrishnan, P.; Saravanakumar, P.; Joshi, N.N.; Harish, B.; Jeyanthi, J. Review on indoor air quality in Indianbuildings. *IOP Conf. Ser. Mater. Sci. Eng.* **2021**, *1145*, 012037. [CrossRef]
44. SPS30—PM2.5 Sensor for HVAC and Air Quality Applications SPS30. Available online: https://sensirion.com/products/catalog/SPS30/ (accessed on 13 May 2022).
45. ATMEGA4808 | Microchip Technology. Available online: https://www.microchip.com/en-us/product/ATMEGA4808# (accessed on 30 May 2022).
46. ATmega4808/4809 Data Sheet. Available online: https://onlinedocs.microchip.com/pr/GUID-4E9DA219-611B-4772-B5D3-9ED908198864-en-US-16/index.html?GUID-0E8898B7-7398-4EBA-A96F-7E9353ECE5E4 (accessed on 30 May 2022).
47. ATWINC1510-IC | Microchip Technology. Available online: https://www.microchip.com/en-us/product/ATWINC1510-IC# (accessed on 30 May 2022).
48. Kuncoro, C.B.D.; Permana, A.F.; Asyikin, M.B.Z.; Adristi, C. Smart Wireless Climate Sensor Node for Indoor Comfort Quality Monitoring Application. *Energies* **2022**, *15*, 2939. [CrossRef]